Available online at www.sciencedirect.com
SCIENCE DIRECT®
Journal of Computational Physics 192 (2003) 73–94
JOURNAL OF COMPUTATIONAL PHYSICS
www.elsevier.com/locate/jcp

Non-uniform convergence of finite volume schemes for Riemann problems of ideal magnetohydrodynamics

M. Torrilhon

Seminar for Applied Mathematics, ETH Zurich, Switzerland

Received 5 November 2002; received in revised form 30 June 2003; accepted 4 July 2003

Abstract

This paper presents Riemann test problems for ideal magnetohydrodynamics (MHD) finite volume schemes. The test problems place emphasis on the hyperbolic irregularities of the ideal MHD system, namely the occurrence of intermediate shocks and non-unique solutions. We investigate numerical solutions for the test problems obtained by several commonly used methods (Roe, HLLE, central scheme). All methods turned out to show a non-uniform convergence behavior which may be paraphrased as 'pseudo-convergence': Initially the methods show convergence towards a wrong solution with irregular wave patterns. Only after heavy grid refinement the methods switch to converge to the true solution. This behavior is most pronounced whenever the solution should be unique but its phase space trajectory lies in the vicinity of that of a non-unique solution. We show detailed grid convergence studies and empirical error analysis. The results may be related to similar results for a 2×2 model system and to time dependent investigations of other authors. The non-uniform convergence is expected to be present for any diffusive finite volume method and question the reliability of coarse grid ideal MHD solutions, also in higher space dimensions.

AMS: 65M12; 76W05

Keywords: Hyperbolic partial differential equations; Magnetohydrodynamics; Riemann problem; Finite-volume-methods; Intermediate waves

1. Introduction

The equations of ideal magnetohydrodynamics (MHD) are formed from the Euler equations of gas dynamics and the induction equation for the magnetic field. They describe the flow of an ideal plasma in interaction with a magnetic field. The physics of the MHD system is described for example in [21] or [22]. The equations build a hyperbolic system of partial differential equations. In the following we will consider Riemann problems for the system of ideal MHD. Though the Euler equations are underlying, the hyperbolic properties of the MHD system are considerably more complex in comparison.

E-mail address: manuel@math.ethz.ch.

0021-9991/$ - see front matter
doi:10.1016/S0021-9991(03)00347-4

There are not only more waves corresponding to a larger system, in addition the system is non-strictly hyperbolic with non-convex flux function and the characteristic fields are no longer either genuinely non-linear or linearly degenerated. By virtue of this, the MHD system may admit non-regular waves, like compound waves and overcompressive shocks, so-called *intermediate* waves. It is also known, that uniqueness of solutions is not guaranteed if intermediate waves are taken into account, e.g. [2,22,29].

Intermediate shocks had been abandoned by evolutionary arguments (see [19,22]) in former times. The research of the last decade, however, showed that those waves might be stable under certain conditions. They may be formed numerically from steepening waves [32], are present in numerical calculations [4,34], and even stable in three-dimensional simulations under finite perturbations (see [10,11]). In [17,18] it was shown that they possess a non-linearly stable viscous profile in most cases. Thus they are conditionally stable in a non-linear analysis (see also [23,24]). Nevertheless, very recently it has been argued against non-evolutionary waves, like intermediate shocks, in [15]. Hence, the relevance of these waves is not yet completely clarified.

Besides the discussion on intermediate shocks a vast number of numerical algorithms has been proposed for the solution of ideal MHD equations. Following the general development of schemes for hyperbolic conservation laws, the papers given in [1–9,20,26–28,31,35] are explicitly investigating MHD. Only a few numerical works mention the subject of irregular waves. In [4] a solution consisting of a compound wave is presented which is further investigated in [2]. In [10–13] multi-dimensional solutions with intermediate waves are discussed. But mostly the subject of intermediate waves or even non-unique solutions is completely ignored in numerical papers. This fact might be due to the lack of theoretical clarity and suitable test problems.

In this paper, we present Riemann test problems for ideal MHD obtained from an exact solver and apply several commonly used numerical MHD schemes to them. See Section 4 for a discussion of the schemes used. The test problems are specially designed to investigate the influence of intermediate waves and non-uniqueness on numerical solutions. The exact solutions have been constructed with an exact Riemann solver described in [30], which extends the classical solvers [6,27] to include intermediate waves. In the investigation of the numerical schemes, all methods turned out to have significant difficulties to compute the test problems accurately. In fact, all numerical results exhibit a kind of non-uniform convergence: Up to a certain number of grid points the numerical solution seems to converge to a wrong solution in which irregular wave patterns exist. The error with respect to the exact solution does not decrease for several grid refinements. Instead parts of the solution may be shown to converge to irregular wave patterns which are not present in the analytical solution. However, after a considerably increase of grid points convergence to the true solution is established and all schemes converge to the true solution. This behavior may have an impact on the reliability of higher dimensional calculations which lack high resolution grids. Hence, high resolution becomes most important if the precise wave patterns are either of particular interest or expected to influence the flow.

The test problems which lead to such non-uniform convergence are not restricted to special cases, like initial conditions with anti-parallel magnetic field, but may be found in general settings. We give an example of an initially non-planar Riemann problem, which produces similar numerical failures. The common feature of both test problems is the appearance of a 180° rotational wave inside the wave structure of the solution. This rotational wave makes the Riemann problem non-unique. It turns out that the non-uniform convergence behavior may be interpreted as interference of the solution in a regular domain with a non-regular, non-unique solution which is closeby. These results extend the findings of [16] where a similar behavior is investigated in the case of a model system. The non-uniform viscosity limit of the waves, both in MHD case and in the case of the model system of [16], affects the convergence behavior of numerical schemes. In this paper these effects are reported in detail for the MHD system. In [33] the time dependence of a disturbed intermediate shock wave is investigated. In Section 5 we show that the

results of [33] may be directly connected to the non-uniform convergence of numerical methods presented in the present paper. The results of Section 5 also furnish to confirm the stability considerations given in [23,24].

The paper is organized as follows: In Sections 2 and 3 of the paper we recall the one-dimensional MHD equations and present and discuss the test problems. In Section 4 the results of the numerical schemes are described. We discuss the phenomena and give a detailed empirical error analysis of the pseudo-convergence. In Section 5 explanations are given and afterwards conclusions are drawn. The paper closes with an Appendix A, where tables with exact values for the presented test cases may be found.

2. MHD Riemann problems

2.1. Equations

The variables of ideal magnetohydrodynamics (MHD) are the fields of density ρ, flow velocity $\mathbf{v}$, magnetic field $\mathbf{B}$ and total energy E. In one-dimensional processes the vectorial variables $\mathbf{v}$ and $\mathbf{B}$ are split into their scalar normal components, v_n and B_n, in the direction of the space variable and the two-dimensional transversal parts, $\mathbf{v}_t$ and $\mathbf{B}_t$. If x is the space direction, we have

$$\mathbf{B} = (B_x, B_y, B_z) = (B_n, \mathbf{B}_t) \quad \text{and} \quad \mathbf{v} = (v_x, v_y, v_z) = (v_n, \mathbf{v}_t). \tag{1}$$

The length of $\mathbf{B}_t$ will be denoted by

$$B_t = \|\mathbf{B}_t\|. \tag{2}$$

Due to the divergence condition which has to be imposed on the magnetic field, the normal component B_n has to be constant in space in one-dimensional processes. The remaining seven fields

$$u = (\rho, v_n, \mathbf{v}_t, \mathbf{B}_t, E) \tag{3}$$

build the set of variables for one-dimensional MHD. We consider only ideal gases and the total energy will be substituted by the pressure, which is related to E by

$$E = \frac{1}{\gamma - 1} p + \frac{1}{2}\rho v_n^2 + \frac{1}{2}\rho \mathbf{v}_t^2 + \frac{1}{2}\mathbf{B}_t^2. \tag{4}$$

Note, that in this equation the contribution of the normal field B_n is suppressed. Throughout the calculations of this paper the adiabatic constant γ is set to be $\gamma = 5/3$.

The one-dimensional MHD equations read

$$\begin{aligned}
&\partial_t \rho + \partial_x(\rho v_n) = 0,\\
&\partial_t \rho v_n + \partial_x\left(\rho v_n^2 + p + \tfrac{1}{2}\mathbf{B}_t^2\right) = 0,\\
&\partial_t \rho \mathbf{v}_t + \partial_x(\rho v_n \mathbf{v}_t - B_n \mathbf{B}_t) = 0,\\
&\partial_t \mathbf{B}_t + \partial_x(v_n \mathbf{B}_t - B_n \mathbf{v}_t) = 0,\\
&\partial_t E + \partial_x\left(\left(E + p + \tfrac{1}{2}\mathbf{B}_t^2\right) v_n - B_n \mathbf{B}_t \cdot \mathbf{v}_t\right) = 0.
\end{aligned} \tag{5}$$

The equation for the normal component of the magnetic field reduces to the statement that B_n is also constant in time. Thus, the normal field B_n is considered only as parameter.

We recall that the system (5) is hyperbolic and has the characteristic velocities

$$\begin{aligned} &\lambda_1 = v - c_{\mathrm{f}}, \quad \lambda_2 = v - c_{\mathrm{A}}, \quad \lambda_3 = v - c_{\mathrm{s}}, \\ &\lambda_4 = v, \\ &\lambda_5 = v + c_{\mathrm{s}}, \quad \lambda_6 = v + c_{\mathrm{A}}, \quad \lambda_7 = v + c_{\mathrm{f}}, \end{aligned} \tag{6}$$

which are formed using the fast and slow magnetoacoustic velocities $c_{\mathrm{f,s}}$, and the Alfven velocity c_{A}, given by

$$c_{\mathrm{f,s}} = \sqrt{\frac{1}{2}\left(\frac{B_n^2 + B_t^2}{\rho} + a^2\right) \pm \sqrt{\frac{1}{4}\left(\frac{B_n^2 + B_t^2}{\rho} + a^2\right)^2 - a^2\frac{B_n^2}{\rho}}}, \tag{7}$$

$$c_{\mathrm{A}} = \sqrt{\frac{B_n^2}{\rho}}. \tag{8}$$

Here the usual sound speed of gas dynamics $a = \sqrt{\gamma(p/\rho)}$ is used as abbreviation. Since

$$c_{\mathrm{s}} \leqslant c_{\mathrm{A}} \leqslant c_{\mathrm{f}} \tag{9}$$

the eigenvalues may coincide at special points in the flow. Hence, the system (5) is only *non-strictly* hyperbolic.

2.2. Riemann problems

In a Riemann problem the system (5) is furnished with discontinuous initial conditions in the form

$$u(x, t = 0) = \begin{cases} u^{(1)}, & x < 0, \\ u^{(0)}, & x > 0. \end{cases} \tag{10}$$

In the regular case, the solution of a Riemann problem (10) for the MHD system is governed by seven waves, either discontinuities or rarefaction fans. Each wave is associated to a characteristic velocity in the following way

$$v \pm c_{\mathrm{f}} : \text{fast shock/rarefaction to the right/left}, \tag{11}$$

$$v \pm c_{\mathrm{A}} : \text{rotational discontinuity to the right/left}, \tag{12}$$

$$v \pm c_{\mathrm{s}} : \text{slow shock/rarefaction to the right/left}, \tag{13}$$

$$v : \text{contact discontinuity}. \tag{14}$$

The contact and rotational discontinuities are linear waves.

As mentioned above the normal magnetic field B_n has to be constant

$$B_n^{(0)} = B_n^{(1)} = B_n, \tag{15}$$

and will be prescribed only as parameter additionally to the initial conditions (10). The transversal field $\mathbf{B}_t$, however, may vary from state 0 to state 1. In Fig. 1 we show general initial conditions for the magnetic field. The absolute value as well as the direction of $\mathbf{B}_t$ may be different in both half-spaces. The initial twist angle of the planes of the magnetic fields is denoted by α. We use the following denotation: Whenever the angle α is not an integer multiple of π the initial conditions are called *non-planar*. In a

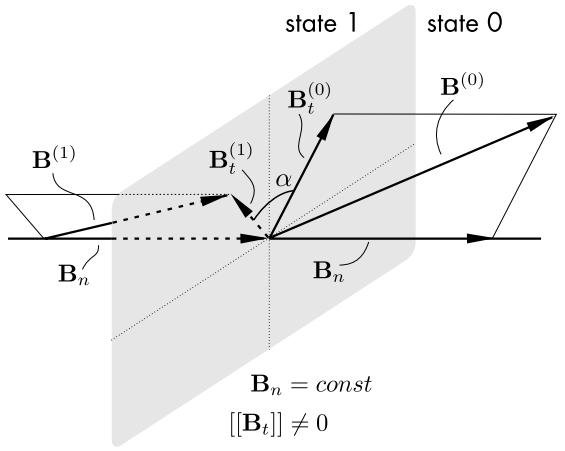

Fig. 1. The initial conditions of a MHD Riemann problem are separated into the constant states 0 and 1. Due to the divergence constraint the normal component of the magnetic field is not allowed to differ in both states. The transversal part may have different absolute values as well as a twist angle α.

non-planar Riemann problem the magnetic fields in state 0 and 1 together with the direction of the space variable define different planes. In the case of α being a integer multiple of π the initial conditions are called *planar*. In the planar case we distinguish between magnetic field vectors pointing in the same ($\alpha = 0$) or in opposite directions ($\alpha = \pi$). The case $\alpha = \pi$, where the magnetic field vectors are anti-parallel is called *coplanar*.

2.3. Solutions of Riemann problems

Analytically, a Riemann problem is solved by assembling shocks and rarefaction waves in an appropriate manner. For the case of ideal MHD the necessary formulas and techniques may be found in [6,27] or [30]. The resulting equations build a non-linear system which has to be solved, e.g. by Newton's method. Thus the solution is not known analytically, but may be calculated numerically to very high accuracy.

Most of the MHD waves form Lax shocks or usual rarefaction waves, which both are called *regular waves* in this paper. However, due to its non-strictness and non-convex flux function the MHD system admits several irregular waves, like overcompressive shocks, so-called intermediate waves, and compound waves.

We shall introduce the following notation: If the solution of a MHD Riemann problem consists only of regular waves, it is called a *r-solution*, i.e. if only Lax shocks or contact discontinuities are present. Otherwise we speak of a *c-solution*, if it contains any non-regular waves like, for instance, compound waves.

Over a wide range of initial conditions the MHD Riemann problem has a regular solution which is unique. Only for certain critical choices (see [29]) of initial conditions the Riemann problem becomes non-unique. In those cases there arises a *c*-solution in addition to the regular solution. One critical choice of initial conditions are coplanar values for the magnetic field and vanishing transversal components of the velocity. The *c*-solution for this case has been observed in [4] and the non-uniqueness was discussed in [2,6]. The structure and constitution of the critical choices and their solutions has been investigated in [29]. For instance, it could be shown that any non-planar Riemann problem with initially vanishing transversal velocities is unique. The critical choices form a hypersurface with one codimension in the space of the initial conditions. Hence, there are initial conditions having only unique *r*-solutions arbitrary close to a critical choice.

Clearly, for calculations with finite volume schemes the non-uniqueness is crucial. What solution the scheme will converge to? In the following section we present classes of test problems to investigate the effect of the non-uniqueness to finite volume schemes.

3. Test problems

The following two classes of initial conditions are both parametrized by the initial twist angle of the transverse magnetic field. Tables with exact values of the solutions may be found in Appendix A.

3.1. Coplanar problem

A possible coplanar Riemann problem is given by the initial conditions (10) with

$$\left(\rho_1, v_n^{(1)}, \mathbf{v}_t^{(1)}, B_n, \mathbf{B}_t^{(1)}, p_1\right) = \left(1, 0, \mathbf{0}, 1, \begin{pmatrix} 1 \\ 0 \end{pmatrix}, 1\right), \tag{16}$$

$$\left(\rho_0, v_n^{(0)}, \mathbf{v}_t^{(0)}, B_n, \mathbf{B}_t^{(0)}, p_0\right) = \left(0.2, 0, \mathbf{0}, 1, \begin{pmatrix} \cos\alpha \\ \sin\alpha \end{pmatrix}, 0.2\right) \tag{17}$$

if the twist angle is set to be $\alpha = \pi$. The velocity vanishes initially and density and pressure have values from a classical shock tube problem. State 1 (state 0) is the high (low) pressure domain. In Fig. 2 four different exact solutions of (16) and (17) are shown in the (B_y, B_z)-plane for increasing values of α. In such a representation each single wave appears as an arc (rotational waves) or a radial line (shocks and rarefactions).

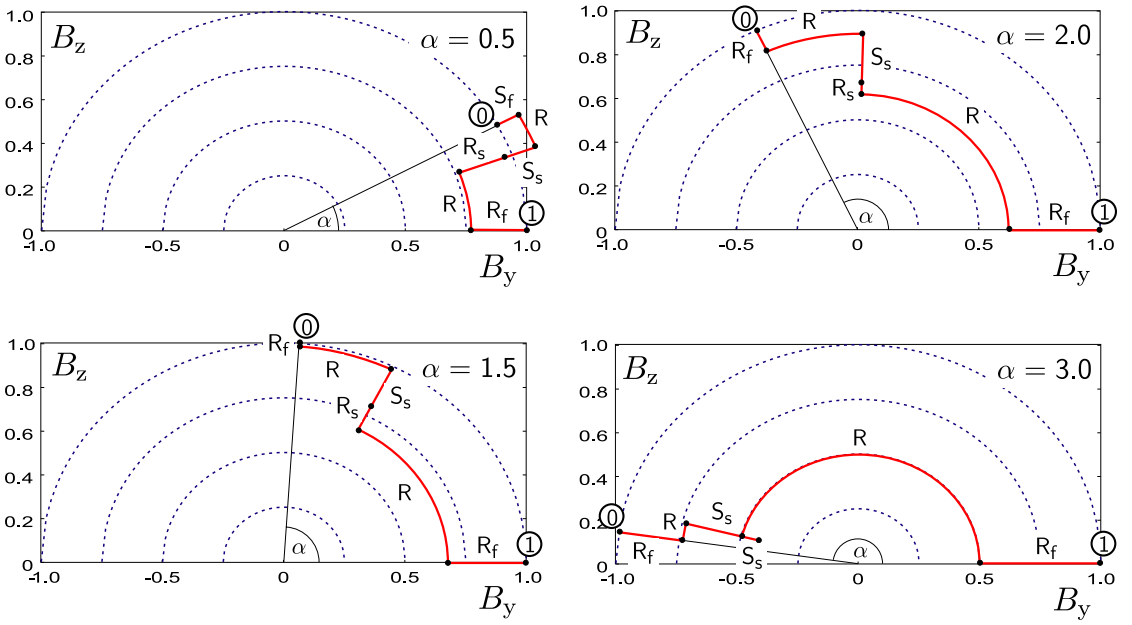

Fig. 2. Exact solutions of Riemann problems with initial conditions (16) and (17) for twist angles $\alpha = (0.5, 1.5, 2.0, 3.0)$. The lines and arcs correspond to fast and slow shocks (S_f/S_s), fast and slow rarefactions (R_f/R_s) and rotations (R). Additionally the initial states 0 and 1 are indicated.

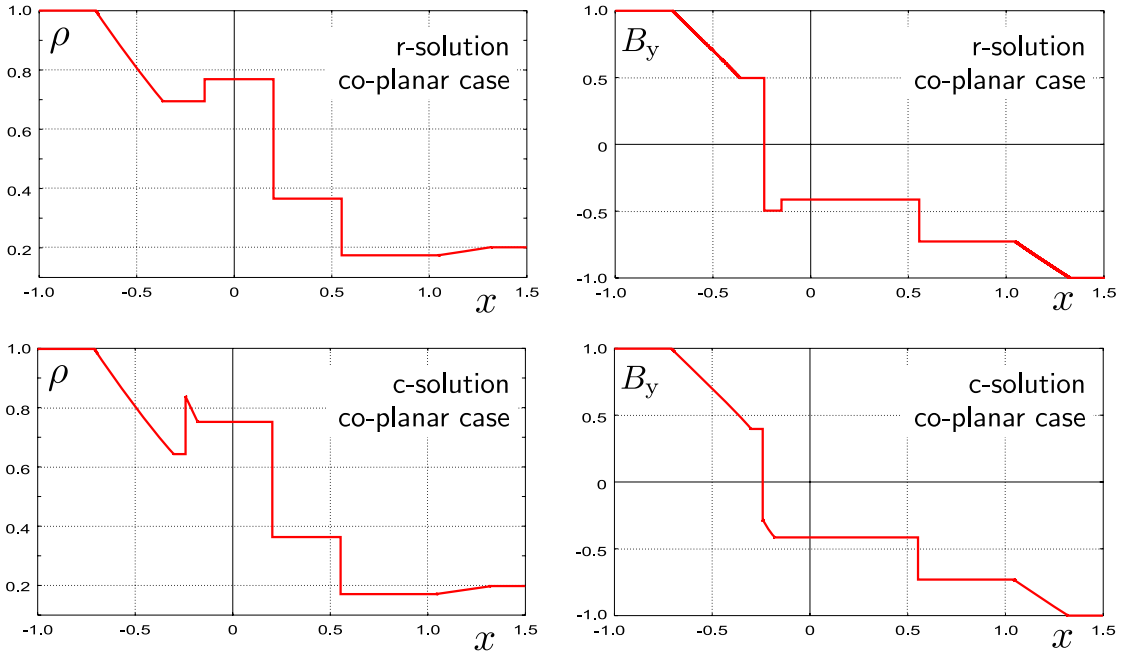

Fig. 3. Comparison of both solutions admissible in the case of the coplanar problem (16) and (17) with $\alpha = \pi$. Upper row: Regular *r*-solution with 180° rotational wave in the magnetic field. Lower row: Irregular *c*-solution with compound wave.

The explicit drawing of lines in case of a shock or a rotational wave is an overstatement. The exact solution, of course, gives only the start and end points of such waves. During the transition $\alpha \to 3.0$ several waves change type. For instance, the fast shock running into state 0 in case of $\alpha = 0.5$ becomes a fast rarefaction in the case $\alpha = 1.5$. All four solutions contain two rotational waves, a left and a right going one.

The solutions shown in Fig. 2 are regular solutions. The solution for $\alpha = 3.0$ is closest to the coplanar case, which is the only critical choice for the initial conditions (16) and (17) if α is varied. In Fig. 3 we display the density and the transverse magnetic field of both coplanar solutions. The *r*-solution contains only one rotational wave (instead of two) which runs into state 1 and "rotates" the transverse magnetic field by an angle of 180°. To be more precise, the rotational wave only changes sign of B_y and $B_z \equiv 0$ holds in the entire solution. The rotational character of the wave may be read off Fig. 2 where the formation of the 180°-rotation is clearly seen. In the irregular *c*-solution the rotational wave and the following slow shock are essentially substituted by a compound wave, i.e. a marginal overcompressive intermediate wave with a slow rarefaction wave attached. A close inspection, however, shows that this substitution also affects the rest of the waves. The values of the density at zero, i.e. behind the contact discontinuity differ by 2%. Also, for the field values behind the right travelling slow shock different values are obtained for the *r*- and *c*-solution. However, this difference is very small, e.g. only 0.4% for the pressure. Nevertheless the *c*-solution should be considered as new independent solution of the Riemann problem.

3.2. Irregular, non-planar problem

In [29] a strategy is described how to construct non-unique, non-planar MHD Riemann solutions. The initial conditions

$$\left(\rho_1, v_n^{(1)}, \mathbf{v}_t^{(1)}, B_n, \mathbf{B}_t^{(1)}, p_1\right) = \left(1.7, 0, \mathbf{0}, 1.1, \begin{pmatrix} 1 \\ 0 \end{pmatrix}, 1.7\right), \tag{18}$$

$$\left(\rho_0, v_n^{(0)}, \mathbf{v}_t^{(0)}, B_n, \mathbf{B}_t^{(0)}, p_0\right) = \left(0.2, 0, \begin{pmatrix} 0 \\ -1.4968909 \end{pmatrix}, 1.1, \begin{pmatrix} \cos\alpha \\ \sin\alpha \end{pmatrix}, 0.2\right) \tag{19}$$

are obtained from this strategy. If the initial twist angle is chosen to be $\alpha = \alpha^\star = 2.4$, the Riemann problem with initial conditions (18) and (19) has a non-unique solution (see below). The possibility to have a non-planar c-solution is realized by an appropriate choice of the initial transversal velocity $\mathbf{v}_t$. The initial values for density, pressure and normal magnetic field are slightly changed in comparison to the coplanar case (16) and (17).

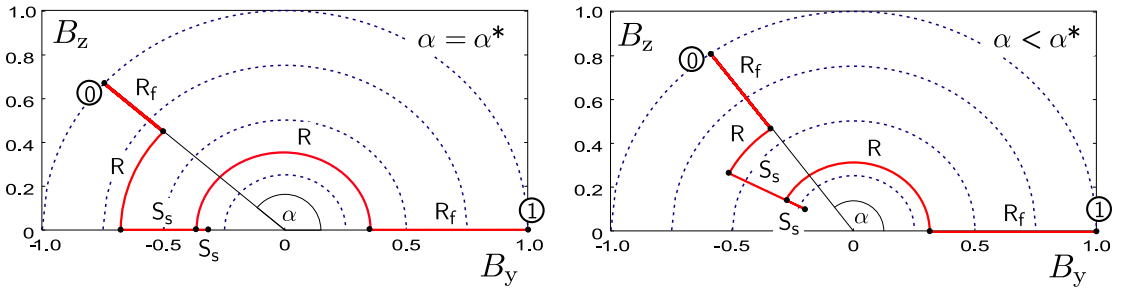

Fig. 4. Exact solutions of Riemann problems with initial conditions (18) and (19) for twist angles $\alpha = \alpha^\star = 2.4$ and $\alpha = 2.2$. The lines and arcs correspond to fast and slow shocks (S_f/S_s), fast and slow rarefactions (R_f/R_s) and rotations (R). Additionally the initial states 0 and 1 are indicated.

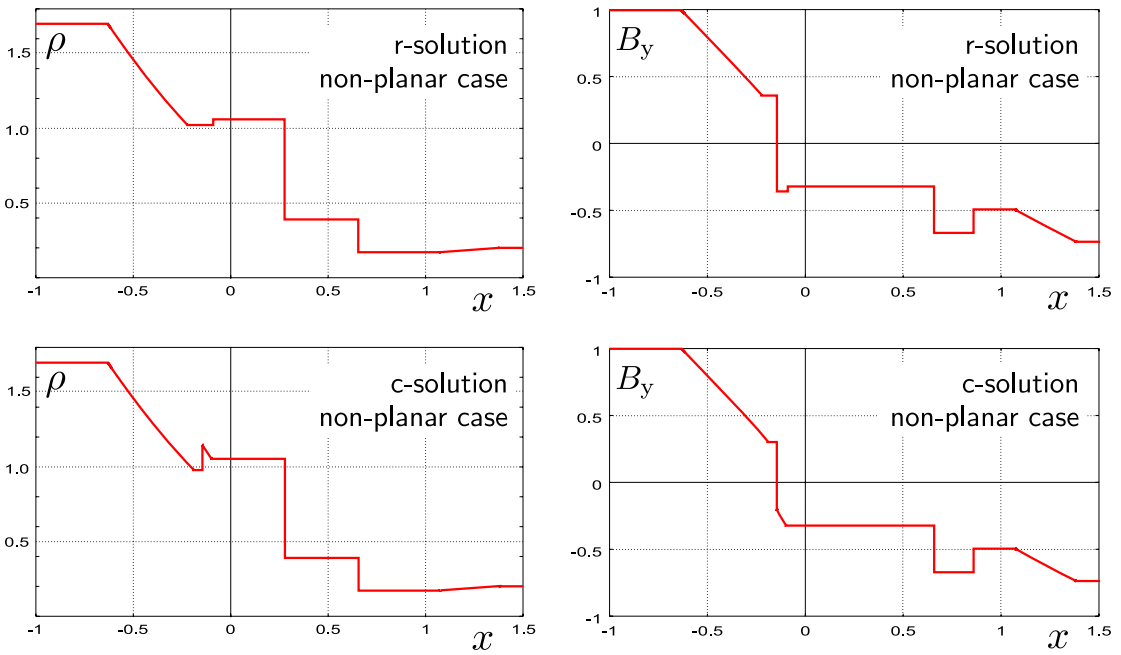

Fig. 5. Comparison of both solutions admissible in the case of the irregular non-planar problem (18) and (19) with $\alpha = 2.4$. Upper row: Regular r-solution with 180° rotational wave in the magnetic field. Lower row: Irregular c-solution with compound wave.

In Fig. 4 the r-solutions for the critical choice $\alpha = \alpha^\star$ and for a regular case $\alpha < \alpha^\star$ are displayed in the (B_y, B_z)-plane. Again the lines for the shocks and rotational waves are overstatements. Both solutions contain two rotational waves, but in the critical case one of them forms a 180° rotational wave. As in the coplanar case this 180° rotational wave is substituted by an intermediate wave in the c-solution. We expect, that any critical choice of initial conditions produces a 180° rotation which leads to the non-uniqueness.

Fig. 5 shows the fields of density and magnetic field B_y for both the r-solution and the c-solution. The r-solution consists of a fast rarefaction, a rotational wave and a slow shock to either sides. Both the c-solution and the r-solution exhibit the same patterns like the solutions in the coplanar case. The 180° rotational wave and the slow shock which travel to the left are substituted by a compound wave. Note, that this non-uniqueness appears in a non-planar setting. In this Riemann problem $B_z \neq 0$ holds in the domain to the right hand side of the right travelling rotational wave.

4. Results

In this section, we solve the coplanar problem as well as the irregular non-planar problem by several finite volume schemes. In addition, we consider Riemann problems with initial conditions close to the critical choices, i.e. $\alpha \approx \alpha^\star$. All results have been obtained in the computational domain

$$x \in [-1, 1.5] \tag{20}$$

with uniform mesh and the end time was chosen to be

$$t_{\text{end}} = 0.4. \tag{21}$$

The different numerical methods are:

- (NT) high resolution central scheme by Nessyahu and Tadmor [25] with ENO limiter and CFL number chosen to be CFL = 0.485.
- (Roe2) high resolution upwind method with approximate Riemann solver after Roe. Uses minmod reconstruction and Runge–Kutta-timestepping with CFL = 0.95. The Roe scheme for MHD was proposed e.g. in [4] and this paper uses an extended version from [31].
- (HLLE) high resolution upwind method with reduced approximate Riemann solver from Harten, Lax, van Leer with MHD extension (see e.g. [14] or [26]). This method uses minmod reconstruction and Runge–Kutta-timestepping with CFL = 0.95.
- (Roe1) first-order Godunov method with Roe-solver. CFL = 0.95.
- (LF) first-order Lax–Friedrichs scheme with CFL = 0.95.

In all cases the limiter is applied to the conservative variables. Furthermore, the results presented in the sequel did not appear to depend on the particular choice of the limiter (ENO/minmod). All schemes, except (NT), has been used in an implementation from Wesenberg [31]. The central scheme was implemented by the author.

4.1. Regular problem

Before we proceed with the irregular problems let us consider the case of a Riemann problem with initial conditions (16) and (17) and twist angle of $\alpha = 0.5$. This Riemann problem is far away from non-uniqueness and irregularities. The solution is computed by (NT) and (Roe2) and compared to the exact solution in order to obtain additional confidence in the implementation of the schemes and the exact solver.

Table 1 shows the L^1-errors of the fields of density and the transverse magnetic field component B_y for both schemes. It has been calculated using

Table 1
L^1-Error study and empirical order of convergence for the two schemes (NT) and (Roe2) in the case of the Riemann problem (16) and (17) with $\alpha = 0.5$

# pts	NT central scheme				Roe-type upwind			
	Error ρ	EOC ρ	Error B_y	EOC B_y	Error ρ	EOC ρ	Error B_y	EOC B_y
50	0.042985		0.035147		0.039788		0.042084	
100	0.022493	0.934	0.017666	0.992	0.023383	0.767	0.026153	0.686
200	0.012430	0.856	0.009475	0.899	0.013884	0.752	0.015521	0.753
400	0.006980	0.832	0.004897	0.952	0.008136	0.771	0.009121	0.767
800	0.003988	0.807	0.002628	0.898	0.004743	0.779	0.005189	0.814
1200	0.002890	0.794	0.001832	0.890	0.003473	0.768	0.003721	0.820
1600	0.002284	0.819	0.001420	0.887	0.002793	0.758	0.002923	0.839
2000	0.001907	0.808	0.001170	0.869	0.002350	0.773	0.002419	0.849
3000	0.001373	0.811	0.000826	0.857	0.001734	0.749	0.001732	0.824
Mean		0.833		0.905		0.765		0.794

Only the fields of density and magnetic field component B_y are displayed. Both schemes show reasonable convergence rates.

$$\mathrm{err}_N = \sum_{i=1}^{N} \Delta x \, \left|\psi_i^{(\mathrm{num})} - \psi^{(\mathrm{ex})}(x_i)\right|, \tag{22}$$

where ψ is the density or the magnetic field component. The empirical order of convergence, also given in Table 1, follows from

$$\mathrm{EOC}_{N_1,N_2} = \frac{\log\left(\frac{\mathrm{err}_{N_1}}{\mathrm{err}_{N_2}}\right)}{\log\left(\frac{N_2}{N_1}\right)} \tag{23}$$

if two errors of successive refined solutions with N_1 and N_2 grid points are given. The results are acceptable for the considered kind of discontinuous problem. Due to the existence of linear waves in the solution, the convergence orders are somewhat smaller then one. Indeed, the parts of the solutions consisting only of shocks or rarefactions exhibit convergence order of unity. The linear waves show convergence orders of only $\frac{3}{4}$. Note that the field of density converges slower then the field of the magnetic field. The reason could be the rather small amplitude of the linear (rotational) waves (see Fig. 2) present in the magnetic field in comparison to a relatively large contact in the density (not shown).

4.2. Almost coplanar problems

The Riemann problem with initial conditions (16) and (17) are now computed for several twist angles $\alpha = (2.8, 2.9, 3.0, 3.1, \pi)$. When approaching the coplanar case all scheme show the same abnormal behavior.

4.2.1. Non-uniform convergence

This subsection discusses the results for $\alpha = 3.0$ which show the most characteristic behavior. We obtained the results of this section with the NT central scheme. However, this scheme is by no means inferior to the other schemes. In fact, the results of any scheme mentioned above would give the same graphs and would differ only slightly in quantitative features. The comparison of the schemes is done in Section 4.2.3.

In Fig. 6 the exact and computed fields of density and magnetic field component B_y are shown for $\alpha = 3.0$. The rest of the fields look correspondingly. In the figure the finite volume computation was based

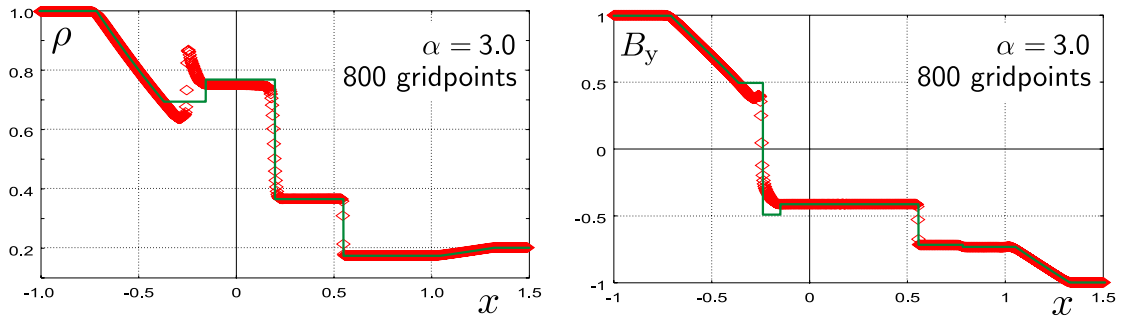

Fig. 6. Numerical and exact solution of the almost co-planar Riemann problem (16) and (17) with $\alpha = 3.0$. The numerical solution uses 800 gridpoints but fails to compute the rotational wave and the slow shock at the right-hand side of the solution.

on 800 grid points ($\Delta x = 3.125 \times 10^{-3}$). The right going slow shock and rarefaction wave are nicely resolved. In the negative half-space, however, the numerical solution fails to compute the rotational wave and the slow shock. Instead, the numerical solution shows the pattern of the compound wave as it would appear in the c-solution of the coplanar problem (see Fig. 3). But this c-solution is not a solution for the case $\alpha = 3.0$, since this case has only a unique r-solution. In this test case the c-solution solves only the case $\alpha = \pi$. Hence, the numerical scheme seems to converge to a wrong solution, at least at the level of 800 grid points.

To investigate this behavior further, the grid is successively refined up to 20,000 points ($\Delta x = 1.25 \times 10^{-4}$). We display the numerical results in Fig. 7 together with the exact solution and the c-solution of the coplanar problem (dotted). For clarity only the interesting interval $[-0.35, -0.1]$ is drawn and the numerical solutions are shown as lines rather than with points. A close look shows that the compound wave pattern starts to break apart between 1600 and 2000 grid points ($\Delta x \approx 1.4 \times 10^{-3}$). With further refinement the density peak shrinks more and more and the shock of the exact solution is very slowly recovered. The magnetic field component B_y exhibits the corresponding behavior: At approximately 1600 grid points the solution starts to approach the amplitude of the rotational wave. Note that for 20,000 grid points the numerical solution is still far off the exact solution. Nevertheless, at last, the exact solution is

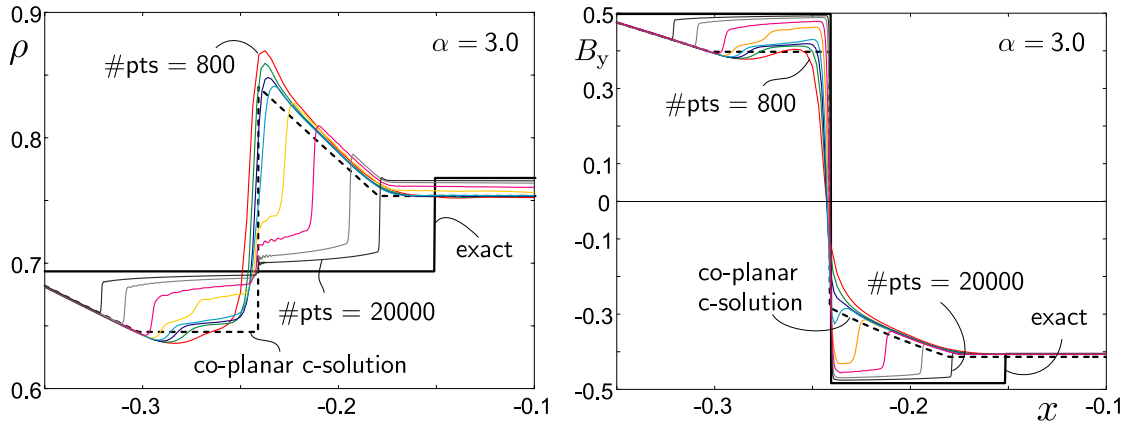

Fig. 7. Convergence study for the Riemann problem (16) and (17) with $\alpha = 3.0$ in the interval $[-0.35, -0.1]$. The eight numerical curves shown refer to 800, 1200, 1600, 2000, 3000, 5000, 10,000 and 20,000 gridpoints. Due to the heavy refinement of the grid the compound wave pattern breaks apart and the exact solution is recovered.

obtained and the convergence is *non-uniform*. The initial convergence to a wrong solution may be referred to as *pseudo-convergence*.

We obtain additional insight by looking at the several numerical solutions in the (B_y, B_z)-plane. The graphs are shown in Fig. 8 which has to be compared to the corresponding picture in Fig. 2. Note that in the viscous setting of the numerical approximation the rotational wave indeed has to rotate the transversal field. That is, there is a strong increase and decrease of B_z over a narrow zone of only several grid points. This is clearly visible in the curve for 20,000 grid points in Fig. 8. The lowest six curves in Fig. 8 correspond to the compound wave patterns which are observed up to 1600 grid points. These curves show already a rotational character. However, the character of this pre-converged wave on coarse grids may not be definitely determined. From the Rankine–Hugoniot-relations of MHD follow that compound waves can only connect states of transverse magnetic fields that lie on a straight line through the origin in the (B_y, B_z)-plane. This is not the case in the figure. Hence, the wave does not fulfill the Rankine–Hugoniot-conditions of a compound wave. On the other hand, a rotational wave does not change the density, as the pre-converged wave does. In [33] intermediate shocks are disturbed by rotational waves and their time dependence is investigated. The time development of the transverse magnetic field in [33] shows basically the same behavior as Fig. 8. In Section 5 we discuss the correspondence of the time dependent intermediate shocks and our grid convergence study in more detail and the temporal interpretation of the above pictures will be explained.

The pictures in Fig. 7 and 8 show essentially the vanishing viscosity limit for the MHD equations which is obtained by grid refinement. That is the numerical method fixed a certain viscosity model and the viscosity tends to zero if the grid is refined. This viscosity limit is known to have irregular properties (e.g. [16–18]). The figures of [16] exhibit a similarity to the plots of the right-hand side of Fig. 7. In [16] a 2×2 model system has been used which mimics the rotational and slow wave family of the MHD equations. For this model system it has been shown in [16] that results like in Fig. 7 may be obtained equivalently by a diffusive numerical method or by adding viscosity to a non-diffusive random choice method. Hence, both results, ours and the results from [16], are consequences of a non-uniform viscosity limit in the case of a degenerate rotational wave whose angle approaches π. Note, that the 2×2 system of [16] models only the behavior of the magnetic field. In the MHD case the non-uniform behavior is present in all other field variables as well. For the density this results in an even stronger disturbance than for the magnetic field: A complete wave is included which breaks apart in the limit, see left-hand side of Fig. 7.

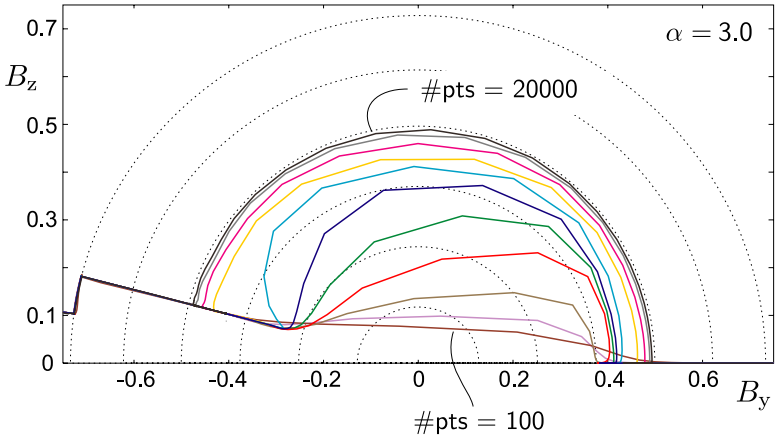

Fig. 8. Convergence study for the Riemann problem (16) and (17) with $\alpha = 3.0$ in the (B_y, B_z)-plane. The eleven numerical curves refer to 100, 200, 400, 800, 1200, 1600, 2000, 3000, 5000, 10,000 and 20,000 gridpoints. Though the first five curves (100–1200 gridpoints) show already rotational character, they represent compound wave patterns.

Up to now we have presented the results for $\alpha = 3.0$. If the twist angle is decreased, the compound wave patterns become less pronounced and the pseudo-convergence cancels at coarser grids. For the case $\alpha = 0.5$ as in Table 1 no pseudo-convergence is observed. However, if α approaches π, ever finer grids are needed to see the compound wave breaking apart. This becomes apparent in the empirical error analysis.

4.2.2. Error analysis

The pseudo-convergence may also be very clearly seen in the error plots of the computed solutions. Therefore, only the interval $[-0.5, 0.0]$ is considered for the calculation of the error. Additionally, it turned out that the error of the field of B_y shows the most significant behavior. The error is computed both with respect to the exact solution and with respect to the c-solution of the coplanar problem. As mentioned already above, this c-solution solves (16) and (17) only for $\alpha = \pi$. Nevertheless, we used the corresponding interval of the c-solution for error computations in order to obtain further insight.

Fig. 9 displays the L^1-errors of solutions with several values of α in (16) and (17) for several grids. The left plot shows the error with respect to the c-solution. All curves, except the last, exhibit a kink representing the refinement at which the compound wave pattern starts to break apart. Up to this point the numerical method showed convergence to a wrong solution with rates between 0.6 and 0.8. But at this point the initial convergence stops and the convergence towards the exact solution is established, which may be seen at the right-hand side of the figure. In this plot, we show the error with respect to the r-solution. In correspondence to the left-hand side convergence is obtained only beyond a certain refinement. Then, convergence rates around 0.6 could be observed, which shows the approximation of the linear rotational wave.

For angles sufficiently different from π the pseudo-convergence vanishes. In contrast, in the limit $\alpha \to \pi$ the convergence towards the c-solution did not stop up to 20,000 grid points. In fact, the c-solution is one of two solutions to the Riemann problem in that case. However, the non-regular waves inside the c-solution are known to be unstable against non-planar perturbations, see e.g. [23,24]. Hence, the following statement seems to be reasonable even though rather theoretical: Due to round-off errors the coplanar initial conditions cannot be *exactly* given in any calculation. Therefore, for a *very* large number of grid points, the compound wave of the coplanar solution would break apart and the r-solution would be recovered also in

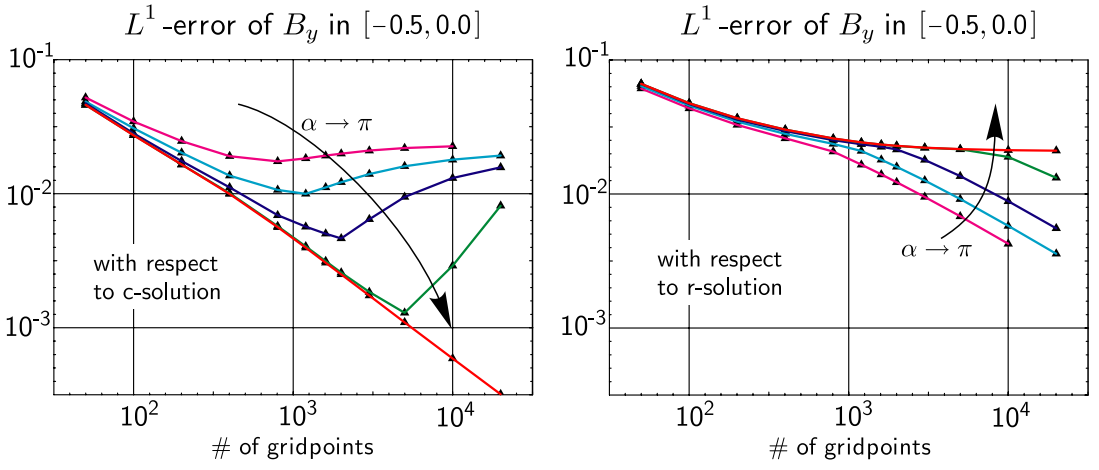

Fig. 9. L_1-Errors for the field B_y of numerical solutions of (16) and (17) calculated on several grids. The value for the twist angle varies $\alpha = (2.8, 2.9, 3.0, 3.1, \pi)$. The left- and right-hand side show the error with respect to the co-planar c-solution and with respect to the exact r-solution.

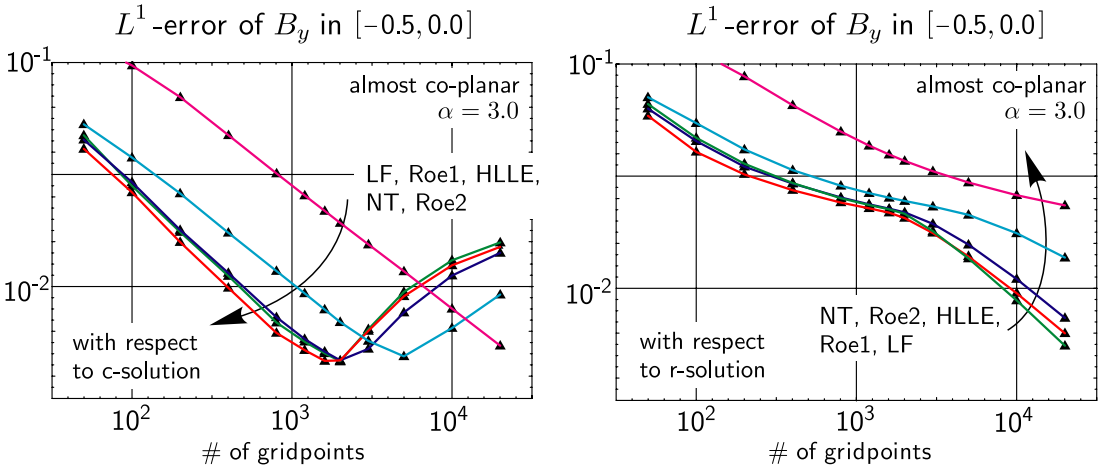

Fig. 10. L_1-Errors for the field B_y of numerical solutions of (16) and (17) calculated on several grids. The value for the twist angle is $\alpha = 3.0$ and the different curve refer to different numerical methods. The left- and right-hand side show the error with respect to the co-planar c-solution and with respect to the exact r-solution.

the case $\alpha = \pi$. The break-down could be accelerated by disturbing the solution in a non-planar way as has been done in [2]. However, analytically the c-solution is a vanishing viscosity solution in the case $\alpha = \pi$, see [16].

4.2.3. Other schemes

All numerical schemes considered exhibit the same pseudo-convergence behavior up to quantitative features. To give an impression we present the errors of the numerical solution of (16) and (17) with $\alpha = 3.0$ for all schemes in Fig. 10. As in Fig. 9 only the interval $[-0.5, 0.0]$ and the errors of B_y are considered. Again the error is calculated with respect to the c-solution as well as with respect to the r-solution. The differences of the schemes are reflected in the degree of refinement which is required to stop the initial convergence towards the c-solution. Since the viscosity is the essential quantity that influences the break-down of the compound wave, the differences of the schemes are directly connected to the different amount of numerical viscosity. Indeed the most diffusive scheme (LF) still shows convergence towards the c-solution at 20,000 grid points. (HLLE) and (Roe1) are more diffusive than (Roe2) and (NT), so they show pseudo-convergence up to finer grids. It is known from the non-uniform viscosity limit that in the case of MHD differences in the viscosity model would lead to different vanishing viscosity limits. Clearly different numerical methods incorporate different artificial viscosity models. However, all numerical schemes considered here show qualitatively the same convergence behavior. We conclude that the differences in the schemes do not influence the non-uniform convergence, at least not for the test problem presented.

The test problems could also be calculated with the MHD scheme of Dai and Woodward [8] as presented in [31]. The resulting graphs and errors for the considered problems were not distinguishable by eye from results of the (Roe2) method. Hence, we omitted the (DW) results in the figure above.

4.3. Almost irregular, non-planar problems

The behavior of the numerical schemes described above is not restricted to almost coplanar problems. Indeed, the same behavior is observed for the non-planar test problem (18) and (19) if the twist angle α is chosen in the vicinity of the critical choice $\alpha^\star$. The following results have been obtained with (Roe2).

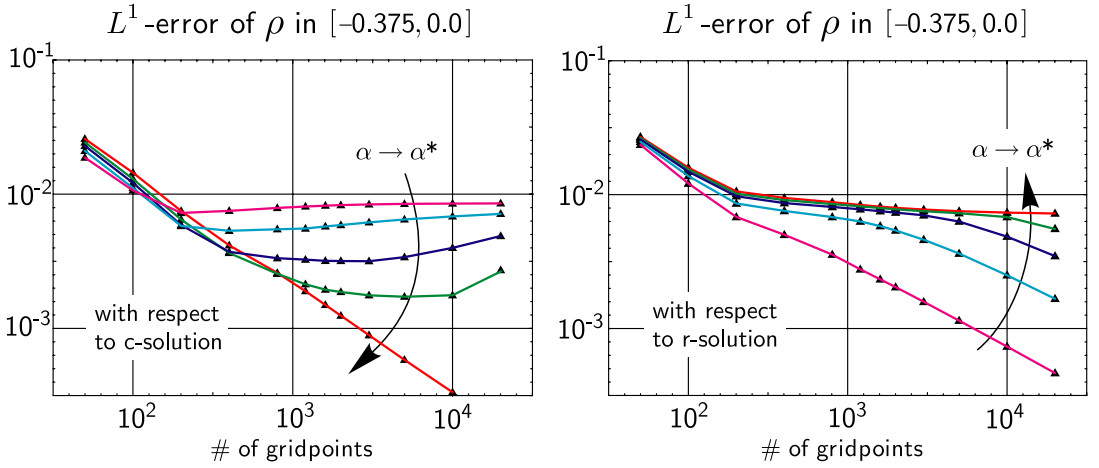

Fig. 11. L_1-Errors for density ρ of numerical solutions of the non-planar problem (16) and (17) calculated on several grids. The value for the twist angle varies $\alpha = (2.0, 2.1, 2.2, 2.3, 2.4)$. The critical choice for this problem is $\alpha^\star = 2.4$. The left-hand side and right-hand side figure show the error with respect to the c-solution of the problem $\alpha = \alpha^\star$ and with respect to the exact r-solution, respectively.

The other schemes give similar results, again depending on the amount of diffusion they introduce in the solution. As in Fig. 6 a compound wave pattern arises in numerical solutions of initial conditions which should only contain regular waves ($\alpha \neq \alpha^\star$). Like in the coplanar problem an *almost* 180° rotational wave which is present for $\alpha \approx \alpha^\star$ is spoiled by compound wave pattern. Only heavy grid refinement make the regular waves appear. The resulting picture for the almost irregular, non-planar case is similar to Fig. 7.

In Fig. 11 we see the errors of the numerical solutions of the irregular, non-planar problem with different choices of α for several grids. For the error in this case only the interval $[-0.375, 0.0]$ and the density field have been considered. As before the c-solution of the irregular problem ($\alpha = \alpha^\star$) as well as the exact (r-) solution furnished to calculate the error. In analogy to the above test case, in this Riemann problem the c-solution is not a solution for choices $\alpha \neq \alpha^\star$. Finally, both pictures show very much the same features as Fig. 9. The initial convergence towards the c-solution of the irregular problem breaks down for a certain refinement and convergence towards the exact solution is established.

Here, the break-down is less pronounced, probably due to the rather weak compound wave in the exact solution (see Fig. 5). The problem with $\alpha = \alpha^\star$ shows convergence towards the c-solution up to 20,000 grid points. Like in the coplanar case we expect the r-solution to appear at very fine grids due to round-off errors which introduce a deviation from $\alpha = \alpha^\star$.

5. Explanation

As mentioned above the pseudo-convergence is connected with the irregular vanishing viscosity limits of the MHD equations. Figs. 6 and 8 demonstrate the appearance of compound wave like pattern in cases where $\alpha \neq \pi$. However, the waves visible in the figures are not solutions to the Rankine–Hugoniot-conditions since they connect non-planar states. A similar statement holds for the almost irregular non-planar case where again the compound wave pattern connects non-planar states in the cases $\alpha \neq \alpha^\star$. Usually, investigations of viscous profiles (e.g. [18]) consider only compound waves with co-planar end states as required by the Rankine–Hugoniot-conditions.

The observations of this paper suggest that the appearance of compound wave patterns in the solutions $\alpha \neq \pi$ may be explained by the existence of a *close but not yet* possible *c*-solution. If the viscous Riemann solution with $\alpha \approx \pi$ was viewed as a solution trajectory in phase space connecting both initial states, the trajectory of a *c*-solution with $\alpha = \pi$ would be nearby. The results of this paper show that a numerical solution is attracted by a trajectory of a *c*-solution whenever such a trajectory is sufficiently close. And this happens even if the c-trajectory does not connect the appropriate initial states, like in the cases $\alpha \neq \pi$ where the *c*-solution is not a solution. Finally, the solution is released into its true trajectory only by considerably reducing viscosity, i.e. grid refinement. In the language of [16] where a 2×2 model system is investigated the non-uniform convergence is a result of a "subtle competition" between the dynamics, i.e. the angle α given by the initial states which has to be matched, and the decreasing viscosity, which leads to different solutions depending on α, see [16].

An explanation may be obtained by comparison with the results of the time dependent investigation made in [33]. However, before we can use those results we establish a re-interpretation of the plots in Figs. 7 and 8. At first, a basic property of the viscosity solution is recalled.

By construction all numerical schemes considered above incorporate diffusive terms. Hence, they solve not ideal MHD but a viscous approximation

$$u_t^{(\varepsilon)} + f\left(u^{(\varepsilon)}\right)_x = \varepsilon u_{xx}^{(\varepsilon)}. \tag{24}$$

The precise form of the viscous terms may be very complicated and not even known explicitly for several non-linear schemes. Eq. (24) must be considered as a model. The viscosity ε is proportional to some power of the grid size $\varepsilon \sim \Delta x^n$ such that (24) is consistent with the homogeneous system if $\Delta x \to 0$. The solution $u^{(\varepsilon)}$ scales with the viscosity ε as

$$\hat{\boldsymbol{u}}\left(\frac{x}{\varepsilon}, \frac{t}{\varepsilon}\right) := u^{(\varepsilon)}(x,t), \tag{25}$$

which can be seen by multiplication of (24) by ε and a change of variables $x \to x/\varepsilon$ and $t \to t/\varepsilon$. We now consider 'self-similar' flow by introducing the new variable $\xi = x/t$ in the function $\hat{\boldsymbol{u}}$. It follows the definition of yet another function $\tilde{\boldsymbol{u}}$ by

$$\tilde{\boldsymbol{u}}\left(\xi, \frac{t}{\varepsilon}\right) := \hat{\boldsymbol{u}}\left(\frac{x}{\varepsilon}, \frac{t}{\varepsilon}\right). \tag{26}$$

Obviously, this function $\tilde{\boldsymbol{u}}$ still represents the solution of (24). However, due to the special dependencies of $\tilde{\boldsymbol{u}}$ we conclude that the relation

$$\lim_{\substack{\varepsilon \to 0 \\ t \text{ fix}}} \tilde{\boldsymbol{u}}\left(\xi, \frac{t}{\varepsilon}\right) = \lim_{\substack{t \to \infty \\ \varepsilon \text{ fix}}} \tilde{\boldsymbol{u}}\left(\xi, \frac{t}{\varepsilon}\right) \tag{27}$$

holds for the solution of (24) and a certain value of ξ. This is the often stated fact that for (24) the limit $\varepsilon \to 0$ gives the same as $t \to \infty$. However, here we want to emphasis that this relation holds only on rays $\xi = x/t = \text{const}$. The sketch in Fig. 12 clarifies the relation (27). Consider the solution $u^{(\varepsilon)}$ of (24) on the interval Ω_1 at certain fixed time $t = 1$ and the space variable shall be labeled by the rays ξ. If we let $\varepsilon \to 0$ for this setting we obtain a certain limit given by the left hand side of (27). On the other hand, consider a fixed amount of viscosity ε and successive intervals Ω_t at increasing time levels t which follow by tracing the end points of Ω_1 along the rays $x/t = \text{const}$. (see Fig. 12). Any interval Ω_t is covered by the rays ξ independent of the time level t and the solution $u^{(\varepsilon)}|_{\Omega_t}$ is considered as function of ξ rather than of x. If $t \to \infty$, according to (27), this function is the same as the vanishing viscosity limit for a fixed time. The important fact is that both limits are compared at positions given by the rays $\xi = x/t = \text{const.}$, that is, the growing intervals Ω_t are rescaled appropriately.

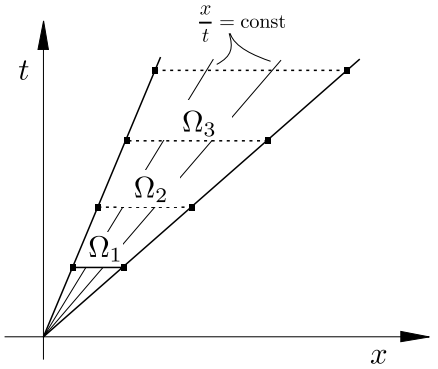

Fig. 12. If a viscosity solution is considered on such rescaled intervals, the viscosity limit $\varepsilon \to 0$ is exchangeable with the time limit $t \to \infty$.

For numerical solutions the relation (27) states that grid convergence studies like in Fig. 7 may be interpreted as *rescaled* time limit of the underlying viscous system. The curves for finer grids now represent later times. Note that in this temporal interpretation the curves are actually rescaled along the rays $x/t = \text{const}$. In the non-scaled space the waves run further to the left with time and also the rotational wave and the slow shock separate more and more and the considered interval becomes larger and larger like in Fig. 12.

The relevance of the time dependent results in [33] now becomes clear. In [33] a certain viscous model for MHD is considered and the viscosity is fixed. For this model the solution is calculated for large times and so-called time dependent intermediate shocks (TDIS) are observed. This calculation corresponds to the right-hand side of (27) while the grid convergence study of this paper calculates the limit at the left-hand side of (27). This explains the significant similarity of the plots given for the TDIS and in Fig. 8. Note, however, that the viscosity model of [33] can not be directly compared to the implicit viscosity introduced by the numerical schemes. Furthermore, the problem in [33] is not a Riemann problem. Nevertheless, a comparison between our results and the results for TDIS remains reasonable. In both cases two states of almost anti-parallel magnetic field vectors are connected by a wave which does not satisfy the Rankine–Hugoniot-conditions, but exhibit a remarkable amount of stability. This wave breaks apart to approach the classical solution only after long times in the case of TDIS, or for fine grids in the calculations of this paper.

The connection established between the pseudo-convergence of MHD schemes and the time dependent intermediate shocks enables us to use the explanation given in [33] in the case of the time dependent behavior for an equivalent explanation of the pseudo-convergence. The key quantity is A_z the integral of the transverse magnetic field components across the compound wave pattern in the (B_y, B_z)-plane, i.e. the area below the curves in Fig. 8. In stationary processes this area is directly related to the integral I_z of $B^{(z)}$ across the compound wave in physical space. Naturally, both quantities are defined only in the viscous setting where a shock is accompanied by certain shock profile. For the following argument we will rely on the area A_z. Like the solution itself $A_z = A_z(t/\varepsilon)$ depends on time and viscosity. According to [33] the quantity $A_z(t/\varepsilon)$ is slowly built up with time in the TDIS with fixed viscosity. The structure of the TDIS breaks apart precisely if A_z reaches a critical value $A_z(t_{\text{crit}}/\varepsilon) = A_z^{(\text{crit})}$ at the time t_{crit}. Afterwards the succeeding wave pattern becomes admissible in the sense that its viscous profile exists, see [33]. Due to the equivalence stated in (27) this fact holds for the convergence behavior as well. Here, we have a fixed time but different grids, that is viscosity ε. At $t_e = 0.4$ on coarse grids, i.e. large viscosity ε, only little $A_z(t_e/\varepsilon)$ is present in the wave structure of Fig. 7, which is evident from Fig. 8. Finer grids result in small viscosity and larger values of A_z are obtained until the marginal value $A_z(t_e/\varepsilon_{\text{crit}}) = A_z^{(\text{crit})}$ is reached at a certain resolution ($\varepsilon_{\text{crit}}$ corresponds

to $\approx$2000 grid points in Fig. 8) and the wave breaks apart. Still the classical waves of the r-solution are not completely established. Like in the case of the TDIS the classical limit is obtained very slowly for large times, or for fine grids, respectively.

In the last section of [24] one finds the statement that "*non-regular waves are not stable for large times but will be needed to describe short time behavior*". To some extent the results of this paper together with the temporal interpretation given by (27) support this statement. In Fig. 7 for small times or coarse grids only the compound wave is visible whereas the rotational waves arises from a certain time on and will be completely formed for large times. This corresponds to the statement given above. However, at this point we have to distinguish between instationary problems like a Riemann problem and a stationary problem. In a Riemann problem the waves may adjust themselves. In a stationary problem with a driving force intermediate waves may be successively rebuilt, see [11].

6. Conclusions

We showed that Riemann solutions of finite-volume-schemes for ideal magnetohydrodynamics are spoiled by wave pattern of irregular Riemann solutions on coarse grids. Only by heavy grid refinement the analytical solution is obtained. In the first place this behavior occurs in the case of initial conditions which have a unique solution with regular waves. The kind of pseudo-convergence appears whenever initial conditions are near by which admit non-unique solutions in which a 180° rotational wave may be substituted by an intermediate wave. In particular, we gave two test examples, with coplanar and non-planar initial conditions which admit such non-uniqueness and study the convergence behavior of several finite volume schemes for these test problems. The results have been correlated to the findings of other authors in other settings. Especially, a close correspondence to the time dependent intermediate shocks of [33] could by established and furnished as explanation of the convergence behavior.

Since any scheme investigated in this paper exhibit essentially the same behavior, we conclude that pseudo-convergence threatens any finite volume simulation of MHD which is based on a diffusive scheme. As has been presented, pseudo-convergence may disappear only at very fine grids or not at all. Hence, special care is recommended when high resolution meshes are not available, like in two or three space dimensions.

To avoid the occurrence of non-uniform convergence in ideal MHD simulations the numerical viscosity has to be minimized as much as possible. It would be worthwhile to test the performance of third or higher order schemes with the presented test problems, though these scheme usually reduce to first order in the vicinity of discontinuities. Alternatively, an adaptive strategy which highly resolves areas with large changes of the direction angle of the magnetic field could help to recover reasonable convergence.

Finally, in the judgment of the pseudo-convergence, it is important to distinguish between ideal and dissipative MHD in this case. The ultimate goal of numerical methods for *ideal* MHD is to converge to the vanishing viscosity solution. This was the case of interest in this paper. Hence, for ideal MHD the irregular wave pattern have to be rejected. However, in the dissipative case they have physical and mathematical significance. Clearly, also in the dissipative case it is desirable for an underlying ideal solver to have proper convergence properties.

Acknowledgements

The author is grateful to Dipl.-math. Matthias Wesenberg from University of Freiburg for generously providing his MHD code for additional comparison of different schemes. Also, the author wishes to thank Dr. Hans De Sterck from University of Colorado at Boulder for very useful suggestions and discussions.

Appendix A. Exact solutions

In the following appendix we give some tables with values of the discussed exact solutions. Only the fields of density and of the transverse magnetic field component B_y are considered. The solutions refer to an end time

$$t_{\text{end}} = 0.4, \tag{A.1}$$

which was chosen for the numerical calculations. For the rarefaction waves only the start and end values are given. In the tables, each row corresponds to a certain wave. The value of the fields gives the state *behind* the wave if one looks at the solution from left to right (from state 1 to state 0).

The complete exact solutions may be obtain by request from the author via E-mail.

A.1. Coplanar problem

Exact values for the *r*-solution of the coplanar Riemann problem with initial conditions (16) and (17) and $\alpha = \pi$:

	x_{start}	x_{end}	ρ (behind)	B_y (behind)
State 1			1.0000000	1.0000000
Rarefaction	−0.7082423	−0.3628142	0.6922069	0.4966783
Rotation	−0.2398390		0.6922069	−0.4966783
Shock	−0.1516145		0.7693119	−0.4137439
Contact	0.2015924		0.3645335	−0.4137439
Shock	0.5517935		0.1725845	−0.7274937
Rarefaction	1.0413879	1.3207457	0.2000000	−1.0000000

Exact values for the *c*-solution of the coplanar Riemann problem with initial conditions (16) and (17) and $\alpha = \pi$:

	x_{start}	x_{end}	ρ (behind)	B_y (behind)
State 1			1.0000000	1.0000000
Rarefaction	−0.7082423	−0.3022800	0.6452294	0.3986243
Shock	−0.2412073		0.8410898	−0.2825269
Attached rarefaction	−0.2412073	−0.1800155	0.7538870	−0.4140819
Contact	0.2036784		0.3653074	−0.4140819
Shock	0.5537568		0.1728151	−0.7300059
Rarefaction	1.0438319	1.3207457	0.2000000	−1.0000000

Exact values for the solution of the almost coplanar Riemann problem with initial conditions (16) and (17) and $\alpha = 3.0$:

	x_{start}	x_{end}	ρ (behind)	B_y (behind)
State 1			1.0000000	1.0000000
Rarefaction	−0.7082423	−0.3646203	0.6936407	0.4994856
Rotation	−0.2405916		0.6936407	−0.4839091
Shock	−0.1513512		0.7682366	−0.4063220
Contact	0.2017165		0.3644655	−0.4063220
Shock	0.5511855		0.1729621	−0.7087891
Rotation	0.7765843		0.1729621	−0.7242827
Rarefaction	1.0453886	1.3207457	0.2000000	−0.9899924

A.2. Irregular, non-planar problem

Exact values of the *r*-solution of the irregular non-planar Riemann problem with initial conditions (18) and (19) and $\alpha = \alpha^\star = 2.4$:

	x_{start}	x_{end}	ρ	B_y
State 1			1.7000000	1.0000000
Rarefaction	−0.6312291	−0.2224215	1.0224315	0.3596119
Rotation	−0.1451486		1.0224315	−0.3596119
Shock	−0.0899376		1.0604288	−0.3225398
Contact	0.2763844		0.3901321	−0.3225398
Shock	0.6544735		0.1708649	−0.6709124
Rotation	0.8556428		0.1708649	−0.4947266
Rarefaction	1.0669255	1.3779391	0.2000000	−0.7373937

Exact values of the *c*-solution of the irregular non-planar Riemann problem with initial conditions (18) and (19) and $\alpha = \alpha^\star = 2.4$:

	x_{start}	x_{end}	ρ	B_y
State 1			1.7000000	1.0000000
Rarefaction	−0.6312291	−0.1912812	0.9796115	0.3026538
Shock	−0.1465035		1.1485298	−0.2013996
Attached rarefaction	−0.1465035	−0.0998446	1.0549708	−0.3226993
Contact	0.2769261		0.3903221	−0.3226993
Shock	0.6549893		0.1709292	−0.6717421
Rotation	0.8559222		0.1709292	−0.4953384
Rarefaction	1.0676406	1.3779391	0.2000000	−0.7373937

Exact values of the solution of the almost irregular non-planar Riemann problem with initial conditions (18) and (19) and $\alpha = 2.3$:

	x_{start}	x_{end}	ρ	B_y
State 1			1.7000000	1.0000000
Rarefaction	−0.6312291	−0.2091904	1.0040806	0.3359741
Rotation	−0.1398621		1.0040806	−0.3288607
Shock	−0.0923658		1.0692932	−0.2658448
Contact	0.2753594		0.3889846	−0.2658448
Shock	0.6609511		0.1672963	−0.6104197
Rotation	0.8401485		0.1672963	−0.4155052
Rarefaction	1.0269580	1.3779391	0.2000000	−0.6662760

References

[1] N. Aslan, Numerical solutions of one-dimensional MHD equations by a fluctuation approach, Int. J. Numer. Methods Fluids 22 (7) (1996) 569.
[2] A.A. Barmin, A.G. Kulikovskiy, N.V. Pogorelov, Shock-capturing approach and non-evolutionary solutions in magnetohydrodynamics, J. Comp. Phys. 126 (1996) 77.
[3] F. Bezard, B. Despres, An entropic solver for ideal Langrangian magnetohydrodynamics, J. Comp. Phys. 154 (1999) 65.
[4] M. Brio, C.C. Wu, An upwind differencing scheme for the equations of ideal magnetohydrodynamics, J. Comp. Phys. 75 (1988) 400.
[5] P. Cargo, G. Gallice, Roe matrices for ideal MHD and systematic construction of Roe matrices for systems of conservation laws, J. Comp. Phys. 136 (1997) 446.
[6] W. Dai, P.R. Woodward, An approximate riemann solver for ideal magnetohydrodynamics, J. Comp. Phys. 111 (1994) 354.
[7] W. Dai, P.R. Woodward, Extension of the piecewise parabolic method to multidimensional ideal magnetohydrodynamics, J. Comp. Phys. 115 (2) (1994) 485.
[8] W. Dai, P.R. Woodward, A simple Riemann solver and high-order Godunov schemes for hyperbolic systems of conservation laws, J. Comp. Phys. 121 (4) (1995) 51.
[9] W. Dai, P.R. Woodward, A high-order iterative implicit-explicit scheme for multidimensional magnetohydrodynamics, SIAM J. Sci. Comput. 19 (6) (1998) 1827.
[10] H. De Sterck, S. Poedts, Intermediate shocks in three-dimensional magnetohydrodynamic bow-shock flows with multiple interacting shock fronts, Phys. Rev. Let. 84 (24) (2000) 5524.
[11] H. De Sterck, S. Poedts, Disintegration and reformation of intermediate shock segments in three-dimensional MHD bow shock flows, J. Geophys. Res. 106 (2001).
[12] H. De Sterck, B.C. Low, S. Poedts, Complex magnetohydrodynamic bow shock topology in field-aligned low-beta flow around a perfectly conducting cylinder, Phys. Plasmas 11 (5) (1998) 4015.
[13] H. De Sterck, S. Poedts, Overcompressive shocks and compound shocks in 2D and 3D magnetohydrodynamic flows, Proc. 8 Int. Conf. Hyperbolic Problems, Intl. Series of Numerical Mathematics 141 (2001) 791.
[14] B. Einfeldt, C.D. Munz, P.L. Roe, B. Sjögreen, On Godunov-type methods near low densities, J. Comp. Phys. 92 (2) (1991) 272.
[15] S.A.E.G. Falle, S.S. Komissarov, On the inadmissibility of non-evolutionary shocks, J. Plasma Phys. 65 (2001) 29.
[16] H. Freistühler, E.B. Pitman, A numerical study of a rotationally degenerate hyperbolic system Part 1: The Riemann problem, J. Comp. Phys. 100 (1992) 306.
[17] H. Freistühler, P. Szmolyan, Existence and bifurcation of viscous profiles for all intermediate magnetohydrodynamic shock waves, SIAM J. Math. Anal. 26 (1) (1995) 112.
[18] H. Freistühler, C. Rohde, Numerical methods for viscous profiles of non-classical shock waves, in: Proc. 7th Int. Conf. Hyp. Problems, Intl. Series of Num. Math., vol. 129, Birkhäuser Verlag, 1999.
[19] A. Jeffrey, T. Taniuti, Non-linear Wave Propagation, Academy Press, New York, 1964.
[20] G.S. Jiang, C.C. Wu, A high-order WENO finite difference scheme for the equations of ideal magnetohydrodynamics, J. Comp. Phys. 150 (2) (1999) 561.
[21] L.D. Landau, E.M. Lifshitz, in: Electrodynamic of Continuous Media, Course in Theoretical Physics, vol. 8, Pergamon Press, Oxford, 1960.
[22] M.A. Liberman, A.L. Velikovich, Physics of Shock Waves in Gases and Plasmas, Springer Series in Electrophysics, vol. 19, Springer, Berlin, 1986.
[23] R.S. Myong, P.L. Roe, Shock waves and rarefaction waves in magnetohydrodynamics. Part 1. A model system, J. Plasma Phys. 58 (3) (1997) 485.

[24] R.S. Myong, P.L. Roe, Shock waves and rarefaction waves in magnetohydrodynamics. Part 2. The MHD system, J. Plasma Phys. 58 (3) (1997) 521.
[25] H. Nessyahu, E. Tadmor, Non-oscillatory central differencing for hyperbolic conservation laws, J. Comp. Phys. 87 (1990) 408.
[26] K.G. Powell, P.L. Roe, T.J. Linde, T.I. Gombosi, D.L. DeZeeuw, A solution-adaptive upwind scheme for ideal magnetohydrodynamics, J. Comp. Phys. 154 (2) (1999) 284.
[27] D. Ryu, T.W. Jones, Numerical magnetohydrodynamics in astrophysics: algorithm and tests for one-dimensional flow, Astrophys. J. 452 (1995) 228.
[28] H.Z. Tang, K. Xu, A high-order gas-kinetic method for multidimensional ideal magnetohydrodynamics, J. Comp. Phys. 165 (1) (2000) 68.
[29] M. Torrilhon, Uniqueness conditions for riemann problems of ideal magnetohydrodynamics, J. Plasma Phys. 69 (3) (2003) 253.
[30] M. Torrilhon, Exact solver for Riemann problems of ideal magnetohydrodynamics, Research report 2002-06, Seminar for Applied Mathematics, ETH Zurich, 2002.
[31] M. Wesenberg, Efficient MHD riemann solvers for simulations on unstructured triangular grids, J. Numer. Math. 10 (2002) 37.
[32] C.C. Wu, Formation, structure, and stability of MHD intermediate shocks, J. Geophys. Res. (space physics) 95 (6) (1990) 8149.
[33] C.C. Wu, C.F. Kennel, Structural relations for time-dependent intermediate shocks, Geophys. Res. Lett. 19 (20) (1992) 2087.
[34] C.C. Wu, Magnetohydrodynamic riemann problem and the structure of the magnetic reconnection layer, J. Geophys. Res. (space physics) 100 (4) (1995) 5579.
[35] A.L. Zachary, A. Malagoli, P. Colella, A higher-order Godunov method for multidimensional ideal magnetohydrodynamics, SIAM J. Sci. Comput. 15 (2) (1994).